

---

---

# Toward Single-Time-Point Image-Based Dosimetry of $^{177}\text{Lu}$ -PSMA-617 Therapy

Julia Brosch-Lenz<sup>1,2</sup>, Astrid Delker<sup>1</sup>, Friederike Völter<sup>1</sup>, Lena M. Unterrainer<sup>1</sup>, Lena Kaiser<sup>1</sup>, Peter Bartenstein<sup>1</sup>, Sibylle Ziegler<sup>1</sup>, Arman Rahmim<sup>2-4</sup>, Carlos Uribe<sup>3,5</sup>, and Guido Böning<sup>1</sup>

<sup>1</sup>Department of Nuclear Medicine, University Hospital, LMU Munich, Munich, Germany; <sup>2</sup>Department of Integrative Oncology, BC Cancer Research Institute, Vancouver, British Columbia, Canada; <sup>3</sup>Department of Radiology, University of British Columbia, Vancouver, British Columbia, Canada; <sup>4</sup>Department of Physics, University of British Columbia, Vancouver, British Columbia, Canada; and <sup>5</sup>Department of Functional Imaging, BC Cancer, Vancouver, British Columbia, Canada

Radiopharmaceutical therapies (RPTs) with  $^{177}\text{Lu}$ -prostate-specific membrane antigen (PSMA) ligands have demonstrated promising results for the treatment of metastatic castration-resistant prostate cancer. The lack of absorbed-dose–effect relationships currently prevents patient-specific activity personalization. To ease the implementation of dosimetry in the routine clinical workflow for RPT, simplified methods such as single-time-point (STP) instead of multiple-time-point (MTP) imaging protocols are required. This work aimed at assessing differences in the time-integrated activity (TIA) of STP versus MTP image-based dosimetry for  $^{177}\text{Lu}$ -PSMA-617 therapy. **Methods:** Twenty metastatic castration-resistant prostate cancer patients with MTP quantitative  $^{177}\text{Lu}$ -SPECT imaging data (~24, 48, and 72 h post injection (p.i.)) available on first and second  $^{177}\text{Lu}$ -PSMA-617 therapy cycles were included in this study. Time–activity curves were fitted for kidneys and lesions to derive effective half-lives and yield a reference TIA. STP approaches involved the formula by Hänscheid (STP<sub>H</sub>) and a prior-information method (STP<sub>prior</sub>) that uses the effective half-lives from the first therapy cycle. All time points were considered for the STP approaches. Percentage differences (PDs) in TIA between STP and MTP were compared for the second therapy cycle. **Results:** Using STP<sub>H</sub> at 48 h p.i. for kidneys showed a  $-1.3\% \pm 5.6\%$  PD from MTP, whereas STP<sub>prior</sub> showed a PD of  $4.6\% \pm 6.2\%$ . The smallest average PDs for the 56 investigated individual lesions were found using STP<sub>prior</sub> at 48 h p.i., at only  $0.4\% \pm 14.9\%$ , whereas STP<sub>H</sub> at 72 h p.i. had a smallest PD of  $-1.9\% \pm 14.8\%$ . **Conclusion:** STP dosimetry for  $^{177}\text{Lu}$ -PSMA-617 therapy using a single SPECT/CT scan at 48 or 72 h p.i. is feasible, with a PD of less than  $\pm 20\%$  compared with MTP. The validity of both STP<sub>H</sub> and STP<sub>prior</sub> has been demonstrated. We believe this finding can increase the adoption of dosimetry and facilitate implementation in routine clinical RPT workflows. Doing so will ultimately enable the finding of dose–effect relationships based on fixed therapy activities that may, in future, allow for absorbed-dose–based RPT activity personalization.

**Key Words:** single-time-point dosimetry;  $^{177}\text{Lu}$ ; PSMA therapy

**J Nucl Med 2023; 64:767–774**

DOI: 10.2967/jnumed.122.264594

**R**adiopharmaceutical therapy (RPT) targeting the prostate-specific membrane antigen (PSMA) has shown significant promise in the treatment of metastatic castration-resistant prostate cancer (mCRPC) (1–3). PSMA radioligand therapy with  $^{177}\text{Lu}$  was first conducted in 2013 (4), and shortly afterward, dosimetry results were reported for  $^{177}\text{Lu}$ -PSMA-617 (5). Considerable improvements in overall survival and radiographic progression-free survival for mCRPC patients receiving  $^{177}\text{Lu}$ -PSMA-617 therapy plus the standard of care, against the standard of care alone in the VISION trial (NCT03511664) (1), led to approval by the U.S. Food and Drug Administration in 2022. Although some evidence of the advantage of dosimetry-based treatment personalization has been shown recently for  $^{90}\text{Y}$  liver radioembolization (6), current practice for most RPTs relies on fixed injected activities. The therapeutic scheme for  $^{177}\text{Lu}$ -PSMA therapy involves 4–6 therapy cycles with fixed activities (7), whereas optimal patient treatment would consider individual factors during RPT planning, such as weight, height, tumor burden, pretreatments, dosimetry, and patients' preferences (8). The lack of broadly available absorbed doses (ADs) for RPT prevents reliable dose–effect relationships for lesions and healthy organs from being obtained, impeding treatment personalization in terms of activity and number of cycles (9). The possibility of correlating pretherapy information with dosimetry and patient outcome was recently shown (10) and should motivate the community to implement routine dosimetry within RPTs and actively plan and adapt an RPT to personalize treatment and maximize patient therapeutic benefit.

The evidence of patient benefit from personalized RPTs is limited by the fact that image-based dosimetry is still not routinely implemented along with RPTs. One limitation preventing clinical adoption of individualized dosimetry is that pharmacokinetic measurements typically require image acquisitions at multiple time points (MTPs) post injection (p.i.) of the radiopharmaceutical. Other factors, such as limited clinical resources (e.g., scanner availability and personnel), as well as the additional costs of MTP imaging and the unclear reimbursement (11), limit the application of personalized dose assessments. This lack of clinical adoption, however, goes against European council directive 2013/79/Euratom, which requests individual planning and verification of exposed target volumes and minimization of dose to nontarget regions, according to the ALARA principle (12).

In this work, we aimed to assess single-time-point (STP) image-based dosimetry for  $^{177}\text{Lu}$ -PSMA-617 therapy for the second therapy cycle. Specifically, we considered the formula by Hänscheid et al.

---

Received Jun. 29, 2022; revision accepted Nov. 14, 2022.

For correspondence or reprints, contact Julia Brosch-Lenz (jbrosch@bccrc.ca).

Published online Jan. 19, 2023.

Immediate Open Access: Creative Commons Attribution 4.0 International License (CC BY) allows users to share and adapt with attribution, excluding materials credited to previous publications. License: <https://creativecommons.org/licenses/by/4.0/>. Details: <http://jnm.snmjournals.org/site/misc/permission.xhtml>.

COPYRIGHT © 2023 by the Society of Nuclear Medicine and Molecular Imaging.

(STP<sub>H</sub>) (13) and a prior-information approach (STP<sub>prior</sub>) that uses MTP imaging during the first therapy cycle and STP imaging for subsequent cycles. We believe that validation of a simple dosimetry approach that requires a single SPECT/CT scan can increase the adoption of dosimetry and facilitate implementation in routine clinical RPT workflows. Doing so can enable the finding of dose–response relationships based on fixed therapy activities that will ultimately allow for AD-based RPT activity personalization.

## MATERIALS AND METHODS

### Patients

This study was conducted on a cohort of patients with mCRPC who received two 6-GBq cycles of <sup>177</sup>Lu-PSMA-617. Twenty patients with MTP imaging data available for both therapy cycles were included. Therapeutic injections and subsequent imaging were performed at the department of nuclear medicine of the university hospital of Ludwig Maximilian University of Munich. Data were irreversibly anonymized. The institutional ethics committee approved this retrospective study (approval 21-0618), and the requirement to obtain informed consent was waived.

### Imaging Protocol

The details of the MTP imaging protocol (Fig. 1) are in the supplemental materials (available at <http://jnm.snmjournals.org>) (5,14–17).

### Determination of Time–Activity Curves

Images were processed using PMOD (version 4.005; PMOD Technologies LLC). The 24 h p.i. SPECT scan of each therapy cycle was chosen as a reference image to which the 48 h p.i. and 72 h p.i. SPECT scans were rigidly registered. Segmentation was performed on the 24 h p.i. SPECT scans of each cycle. The kidneys were segmented by applying a 20% fixed threshold, which produced good alignment when overlying the kidney volumes of interest (VOIs) on the CT scan, excluding the kidney pelvis. Manual adjustments were made when necessary. The qPSMA approach of Gafita et al. (18) was adopted for segmentation of individual lesions on the 24 h p.i. SPECT scan per cycle, which was converted into standardized uptake values (SUVs) based on body weight. The determined patient- and cycle-specific threshold was applied to the 24 h p.i. SPECT scan with an automatic multiregion approach. Physiologic uptake regions that were mistakenly selected as VOIs by the automatic multiregion threshold approach, such as in the gastrointestinal tract or bladder, were removed. Lastly, a whole–field-of-view (FOV) tumor burden (TB<sub>FOV</sub>) VOI containing all individual lesions was created. The lesion segmentation

was verified and, if necessary, manually adjusted on the SPECT and CT scans by 2 experienced readers in a consensus reading.

All VOIs were copied to the coregistered 48 h p.i. and 72 h p.i. SPECT scans, and the activity values of each VOI were extracted to generate time–activity curves. These were fit to a monoexponential function using MATLAB (version R2019b; The MathWorks, Inc.) to determine the effective half-lives ( $T_{1/2\text{ eff}}$ ) (17) for kidneys, TB<sub>FOV</sub>, and individual lesions. The procedure was performed for both therapy cycles.

### Time-Integrated Activity (TIA) with MTP and STP Approaches

The TIA for each VOI in the second therapy cycle was calculated using 3 different methods: the first used the monoexponential fit with all points available from the MTP scans in the second cycle (considered the reference TIA (TIA<sub>ref</sub>), determined from activity at time  $t = 0$  for the second therapy cycle,  $A_0^{2\text{nd}}$ , and  $T_{1/2\text{ eff}}$  for the second therapy cycle,  $T_{1/2\text{ eff}}^{2\text{nd}}$  [Eq. 1]); the second used  $T_{1/2\text{ eff}}$  determined from the curve fitting of the first cycle ( $T_{1/2\text{ eff}}^{1\text{st}}$ , prior information) and the STP activity value of the second cycle; and the third used the approach suggested by Hänscheid (13).

$$\text{TIA}_{\text{ref}} = \frac{A_0^{2\text{nd}}}{\ln 2 / T_{1/2\text{ eff}}^{2\text{nd}}} \quad \text{Eq. 1}$$

Three different STP TIAs were calculated for the second method, STP<sub>prior</sub>, with Equation 2 by combining  $T_{1/2\text{ eff}}^{1\text{st}}$  with the single activities  $A(t)$  measured at time  $t = 24, 48, \text{ or } 72$  h p.i.

$$\text{STP}_{\text{prior}} \text{ TIA} = \frac{A(t) \cdot 2 \cdot \frac{t}{T_{1/2\text{ eff}}^{1\text{st}}}}{\frac{\ln 2}{T_{1/2\text{ eff}}^{1\text{st}}}} \quad \text{Eq. 2}$$

The third method, STP<sub>H</sub>, estimated the STP TIA using the method of Hänscheid (13). This approach assumes that if the imaging time point  $t$  is within the interval from 0.75 to 2.5 times the  $T_{1/2\text{ eff}}$  of the respective VOI, one can replace Equation 2 by a simplified formula (Eq. 3) with less than 10% error in TIA compared with MTP. Three different STP TIAs were calculated using the activities  $A(t)$  measured at time  $t = 24, 48, \text{ or } 72$  h p.i.

$$\text{STP}_{\text{H}} \text{ TIA} \approx \frac{A(t) \cdot 2 \cdot t}{\ln 2} \quad \text{Eq. 3}$$

### Comparisons

The STP approaches for the second therapy cycles were compared with the MTP reference. The percentage difference (PD) in STP TIA versus TIA<sub>ref</sub> was calculated for each kidney, for TB<sub>FOV</sub>, and for up to 6 lesions

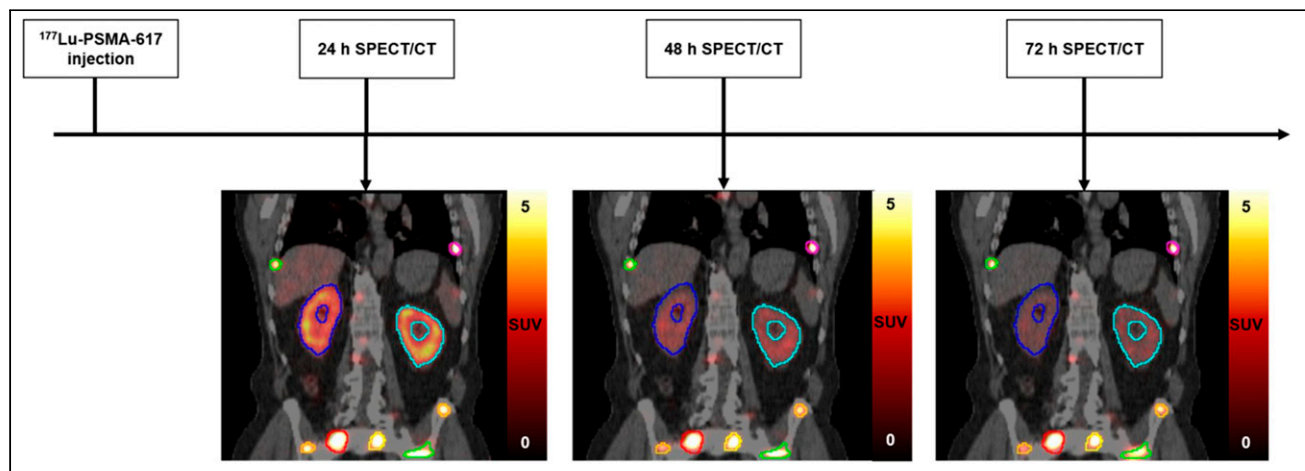


FIGURE 1. Overview of MTP imaging protocol.

per patient if they were visible in the FOV of both cycles. Bland–Altman plots were used to compare the STP approaches with MTP (19,20).

### Statistical Analyses

Statistical analysis used the Wilcoxon signed-rank test for comparisons between MTP and each STP approach and between the  $T_{1/2\text{ eff}}$  of the first and second cycles.

### RESULTS

Unless otherwise stated, all reported values are given as average  $\pm$  SD (minimum; maximum).

### Patients

Twenty patients with mCRPC were included in this analysis. The average administered activity of  $^{177}\text{Lu-PSMA-617}$  for all patients and therapy cycles was  $6.09 \pm 0.13$  GBq (5.74; 6.70 GBq). Left and right

kidneys were analyzed separately. The patients'  $\text{TB}_{\text{FOV}}$  volume averaged  $462 \pm 361$  ml (8; 1,229 ml). One patient had no lesions within the SPECT FOV. In total, 56 lesions that were seen within the FOV for the first and second therapy cycles were analyzed.

### Distribution of Effective Half-Lives

Figure 2 shows the  $T_{1/2\text{ eff}}$  distributions obtained with the MTP approach. The average  $T_{1/2\text{ eff}}$  for the first and second therapy cycles was  $32.5 \pm 7.0$  h (17.8; 51.9 h) and  $31.7 \pm 6.4$  h (21.6; 45.7 h), respectively, for kidneys;  $75.3 \pm 41.8$  h (45.5; 240.0 h) and  $64.8 \pm 35.0$  h (14.5; 192.8 h), respectively, for  $\text{TB}_{\text{FOV}}$ ; and  $69.0 \pm 40.0$  h (20.1; 249.7 h) and  $66.6 \pm 34.2$  h (19.7; 216.2 h), respectively, for individual lesions. Twenty-six of the 56 investigated lesions had a  $T_{1/2\text{ eff}}$  PD of more than  $\pm 20\%$ .

When  $T_{1/2\text{ eff}}$  obtained with the MTP approach was compared between the first and second therapy cycles using the Wilcoxon

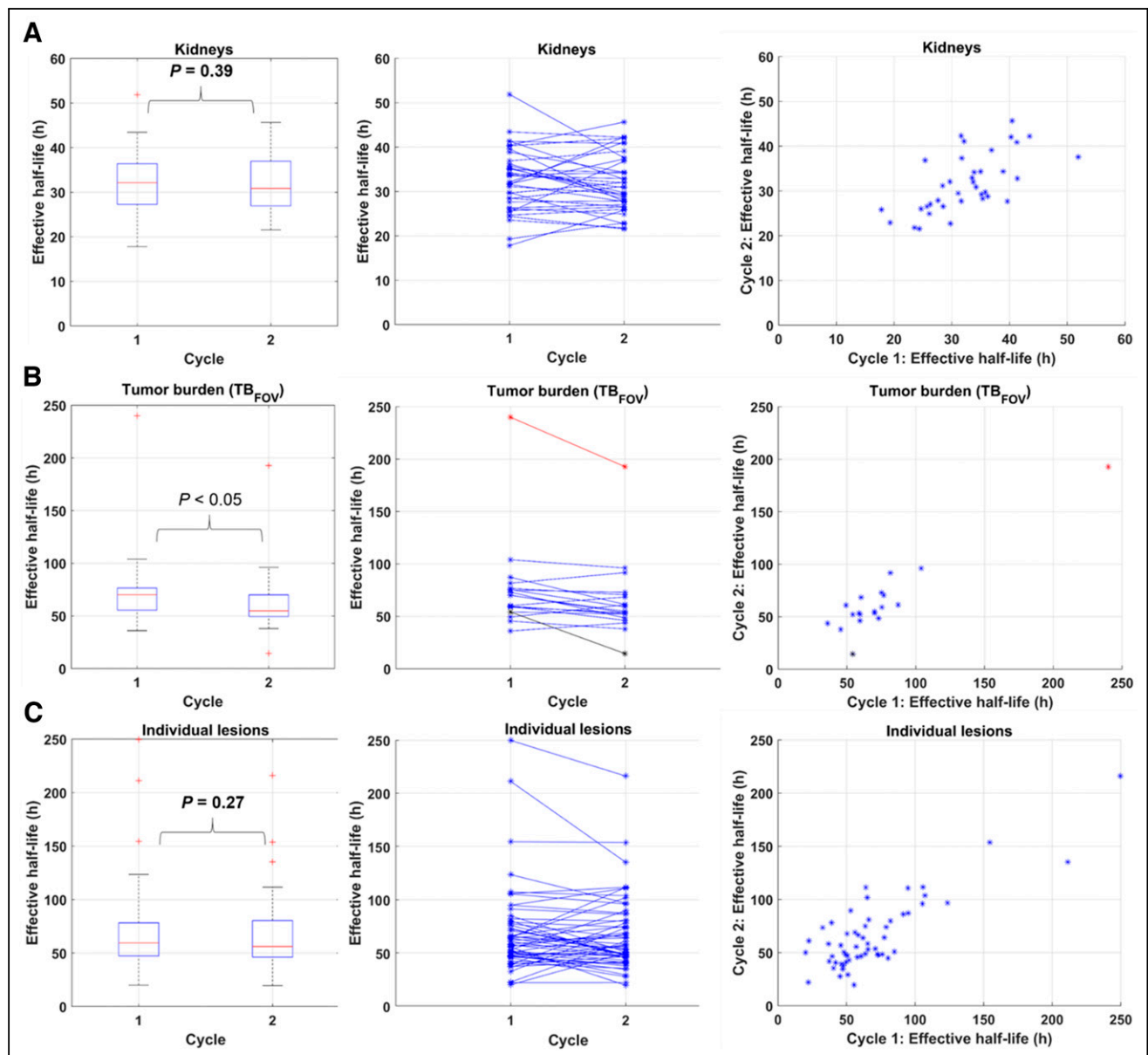


**FIGURE 2.** Distribution of  $T_{1/2\text{ eff}}$  calculated using MTP method for kidneys (A),  $\text{TB}_{\text{FOV}}$  (B), and individual lesions (C) for both therapy cycles. Plots further include results of statistical analysis using Wilcoxon signed-rank test for  $T_{1/2\text{ eff}}$  between cycles 1 and 2.

signed-rank test, significant differences (i.e.,  $P < 0.05$ ) were found for  $TB_{FOV}$  ( $P = 0.02$ ) ( $n = 19$ ; 1 patient had no lesions) but not for kidneys ( $P = 0.39$ ) ( $n = 37$ ; 3 patients had only 1 active kidney) or individual lesions ( $P = 0.27$ ) ( $n = 56$ ).

### Comparison of TIA with Respect to STP Approaches

Figure 3 shows the PDs in TIA between the MTP and STP approaches. Supplemental Table 1 displays the values.

The Bland–Altman plots of  $STP_{prior}$  and  $STP_H$  compared with MTP are given in Figures 4 and 5. The mean relative difference between MTP and  $STP_{prior}$  was closest to zero for kidneys at 24 h p.i., for  $TB_{FOV}$  at 72 h p.i., and for individual lesions at 48 h p.i. (Fig. 4). However, the limits of agreement were smallest for kidneys at 48 h p.i., for  $TB_{FOV}$  at 72 h p.i., and for individual lesions at 48 h p.i. For  $STP_H$ , the difference from MTP was closest to zero, with the smallest limits of agreement at 48 h p.i. for kidneys and at 72 h p.i. for individual lesions (Fig. 5). For  $TB_{FOV}$ , the difference was smallest at 72 h p.i., whereas the limits of agreements were slightly smaller at 48 h p.i.

### Statistical Analyses

The results of the statistical analysis for the STP approaches compared with the MTP reference are shown in Figure 3. In general, no significant difference in TIA for kidneys was found for an  $STP_{prior}$  at 24 h p.i. or an  $STP_H$  at 48 h p.i. For  $TB_{FOV}$ , no significant difference in TIA was found for an  $STP_{prior}$  at 48 h p.i. or  $STP_H$  at 72 h p.i. Lastly, for individual lesions, no significant difference in TIA was

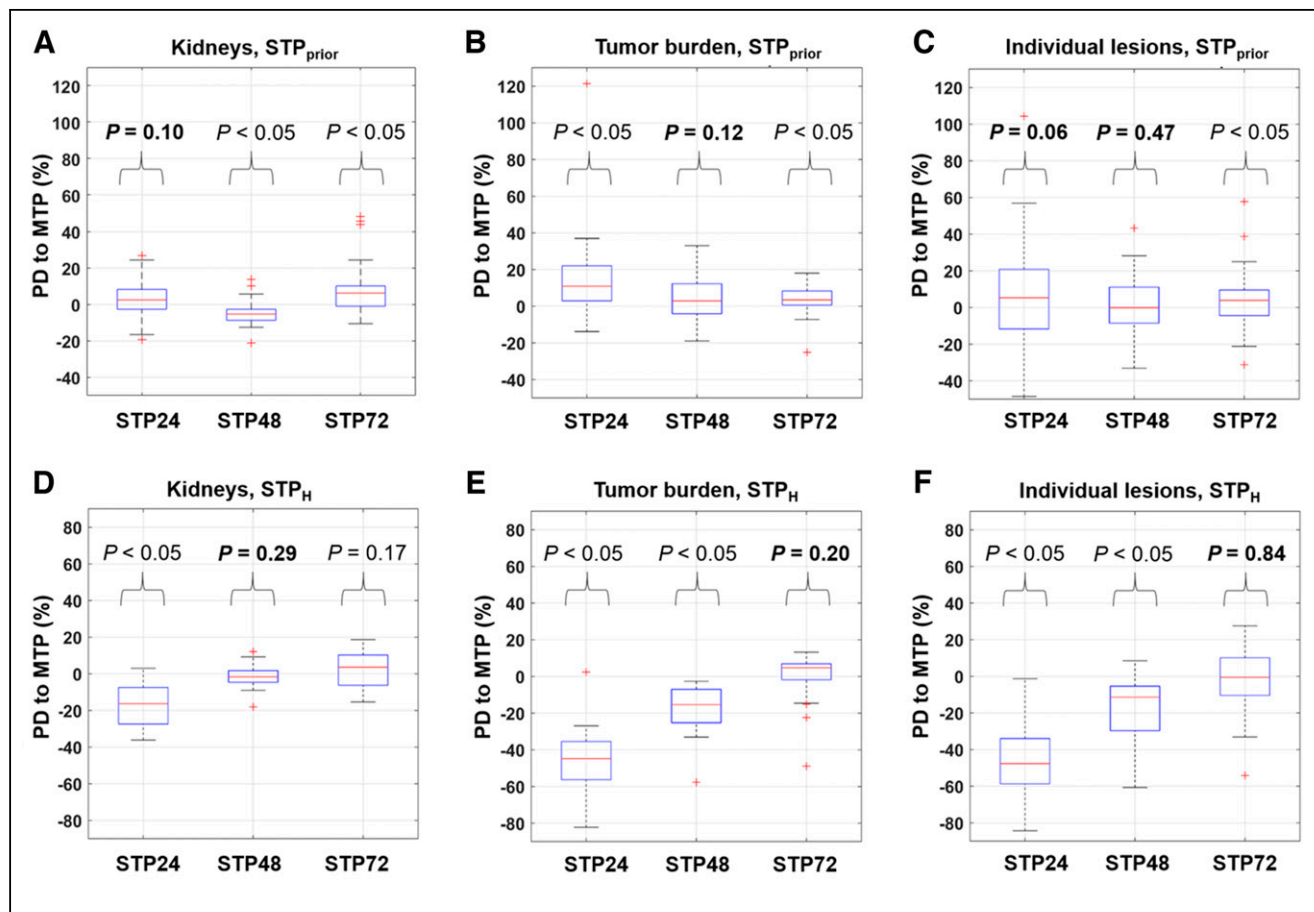
found for an  $STP_{prior}$  at 24 h p.i.,  $STP_{prior}$  at 48 h p.i., or  $STP_H$  at 72 h p.i.

Table 1 summarizes the number and percentage of VOIs for which the imaging time points per therapy cycle were within the interval from 0.75 to 2.5 times the  $T_{1/2\text{eff}}$  of that region as calculated with the MTP approach. The imaging time point at 48 h p.i. lay within that range for 97% and 100% of kidneys for both cycles 1 and 2, whereas for  $TB_{FOV}$  and individual lesions, the largest number of VOIs within that range was at 72 h p.i. However, for 25% of individual lesions and 21% of the  $TB_{FOV}$  VOIs, 72 h p.i. was outside the interval for cycle 2.

Figure 6 shows the percentage of VOIs for which the STP TIA was within  $\pm 10\%$  and  $\pm 20\%$  of  $TIA_{ref}$  for both the  $STP_{prior}$  and  $STP_H$  approaches. For  $STP_H$ , 95% of kidneys were within  $\pm 10\%$  of  $TIA_{ref}$  at 48 h p.i., compared with 86% for  $STP_{prior}$ . For  $TB_{FOV}$ , 95% of VOIs were within  $\pm 20\%$  of  $TIA_{ref}$  at 48 h p.i. and 72 h p.i. for  $STP_{prior}$ , compared with 68% and 89% for  $STP_H$ , respectively. For  $STP_{prior}$ , 86% and 91% of the individual lesions were within  $\pm 20\%$  of  $TIA_{ref}$  at 48 h p.i. and 72 h p.i., compared with 63% and 86% for  $STP_H$ , respectively.

### DISCUSSION

In this work, we aimed at comparing STP with MTP image-based dosimetry methods, which could increase clinical adoption. STP dosimetry methods have been studied predominantly for



**FIGURE 3.** Distribution of PD of TIA in  $STP_{prior}$  (A–C) and  $STP_H$  (D–F) vs. MTP reference for kidneys (A and D),  $TB_{FOV}$  (B and E), and individual lesions (C and F). Plots further include results of statistical analysis using Wilcoxon signed-rank test between MTP and each respective STP approach.

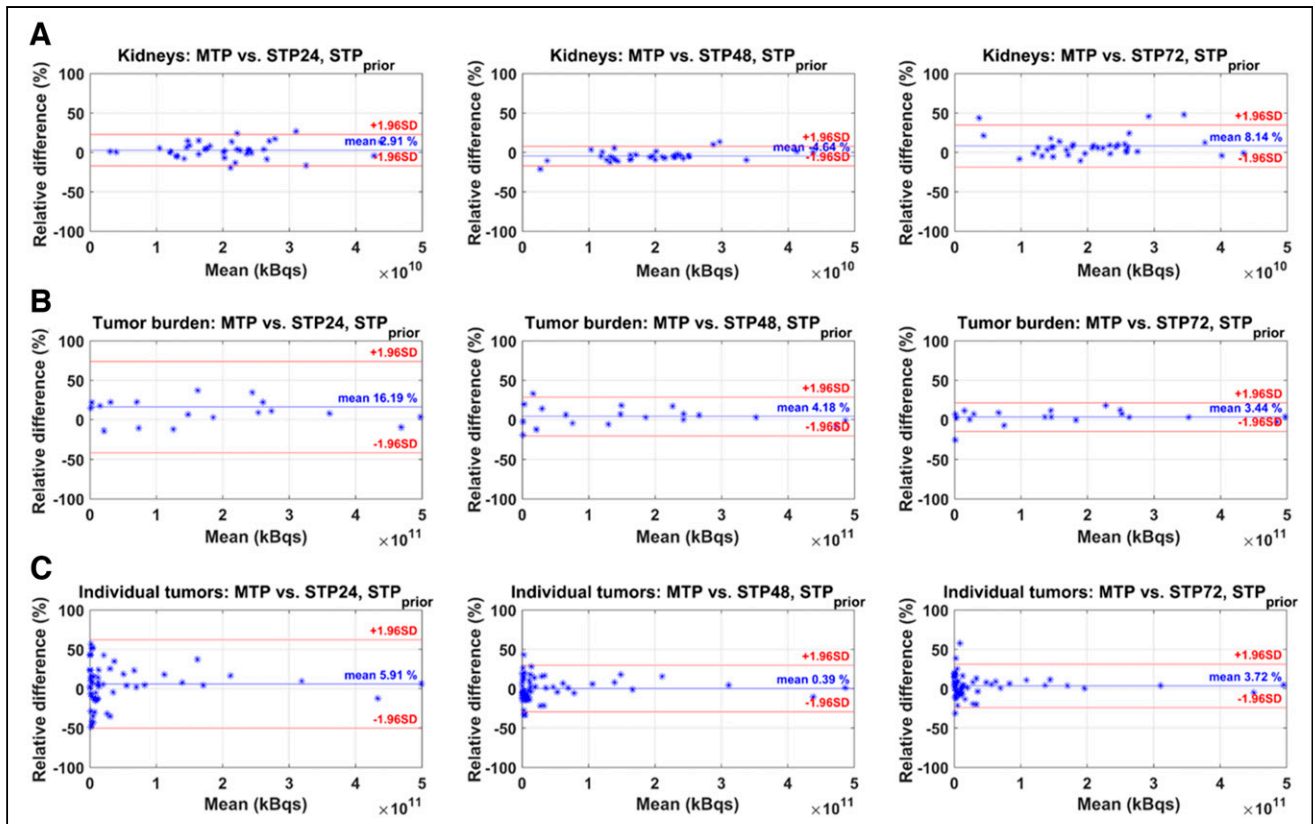


**FIGURE 4.** Bland–Altman plots of  $STP_{prior}$  vs. MTP reference for kidneys (A),  $TB_{FOV}$  (B), and individual lesions (C).  $STP_{24}$  = STP at 24 h p.i.;  $STP_{48}$  = STP at 48 h p.i.;  $STP_{72}$  = STP at 72 h p.i.

$^{177}\text{Lu}$ -DOTATATE therapy (13,21–23) but also for  $^{177}\text{Lu}$ -PSMA therapy (24–26). Three different approaches for STP dosimetry have been proposed: population-based mean  $T_{1/2\text{ eff}}$  (27), using prior information from the first therapy cycle for subsequent cycles (26), and using the formula by Hanscheid et al. (13). The first approach has been suggested to be valid for calculation of kidney ADs in  $^{177}\text{Lu}$ -DOTATATE and  $^{90}\text{Y}$ -DOTATOC therapies (22,27). Given the mean  $T_{1/2\text{ eff}}$  of  $32.5 \pm 7.0$  h p.i. and  $31.7 \pm 6.4$  h p.i. for the first and second  $^{177}\text{Lu}$ -PSMA-617 therapy cycles determined from MTP imaging in this work, this approach may be a valid assumption. However, given the high variation and large spread of  $T_{1/2\text{ eff}}$  for  $TB_{FOV}$  and individual lesions (Figs. 2B and 2C), the population-based approach may not be suitable for lesion AD calculations in  $^{177}\text{Lu}$ -PSMA therapies. Therefore, we compared clinically feasible dosimetry approaches for kidneys and lesions with a reduced number of imaging time points based on  $STP_{prior}$  and  $STP_H$ .

$STP$ -based approaches showed smaller differences between TIA and  $TIA_{ref}$  for kidneys than for lesions. These differences can be associated with the smaller variations in  $T_{1/2\text{ eff}}$  (Fig. 2). For the  $STP_{prior}$  approach, our analysis indicated that an STP at 24 h p.i. results in TIA differences from MTP that are on average closer to zero (Fig. 3A). However, 48 h p.i. is more favorable if a smaller range of variations in PD versus  $TIA_{ref}$  is preferred (Figs. 3A and 4A). Our results agree with those reported by Kurth et al. (26), who applied the  $STP_{prior}$  approach for cycles 2–6 and found differences in AD of  $\pm 6\%$  for kidneys and  $\pm 10\%$  for parotid glands when using a single SPECT scan at 48 h p.i. of  $^{177}\text{Lu}$ -PSMA-617, compared with MTP. Our analysis also suggests that when using

the  $STP_H$  approach, an STP at either 48 h p.i. or 72 h p.i. is favorable. However, an  $STP_H$  at 48 h p.i. may be optimal for kidney AD calculations given the smaller range of variations in STP TIA versus  $TIA_{ref}$  (Figs. 3B and Fig. 5A). For kidneys,  $STP_H$  outperformed  $STP_{prior}$  at 48 h p.i. in terms of PD in TIA with respect to MTP (Fig. 6). With  $STP_H$ , most (95%) kidney TIAs are expected to be within 10% of those calculated with MTP, with few (5%) falling within 10%–20%. For all kidneys except one, the 48 h p.i. imaging time point was within the interval from 0.75 to 2.5 times the  $T_{1/2\text{ eff}}$ .  $STP_H$  therefore yielded TIA estimates very close to  $TIA_{ref}$ .  $STP_{prior}$ , on the other hand, relies on a comparable  $T_{1/2\text{ eff}}$  for cycles 1 and 2. We observed up to a 45% difference in  $T_{1/2\text{ eff}}$  for some investigated kidneys. However, this translated to a PD in  $TIA_{ref}$  of between only  $-6\%$  and  $14\%$ , which could be tolerated as long as the overall kidney function of the patient was good before therapy and the cumulative kidney AD was far below the considered toxicity threshold of 23 Gy.

For  $TB_{FOV}$  and individual lesions, an imaging time point of 72 h p.i. seems optimal, as the ranges of PD when compared with MTP are the smallest (Figs. 3A, 4B, and 4C) for the  $STP_{prior}$  approach. Similarly for  $STP_H$ , the PD when compared with MTP was closer to zero at 72 h p.i. (Figs. 3B, 5B, and 5C). However, to obtain TIA estimates for both kidneys and lesions in a single scan, an STP at 48 h p.i. might be a valid compromise. But this compromise comes at a higher variation in PD with respect to MTP for lesions.

$STP_{prior}$  performed better overall for  $TB_{FOV}$  and individual lesions than did  $STP_H$  (Fig. 6). The performance of  $STP_H$  improved with later imaging time points. This finding agrees with findings reported by Hanscheid et al. for  $^{177}\text{Lu}$ -DOTATATE (13) and Jackson et al.

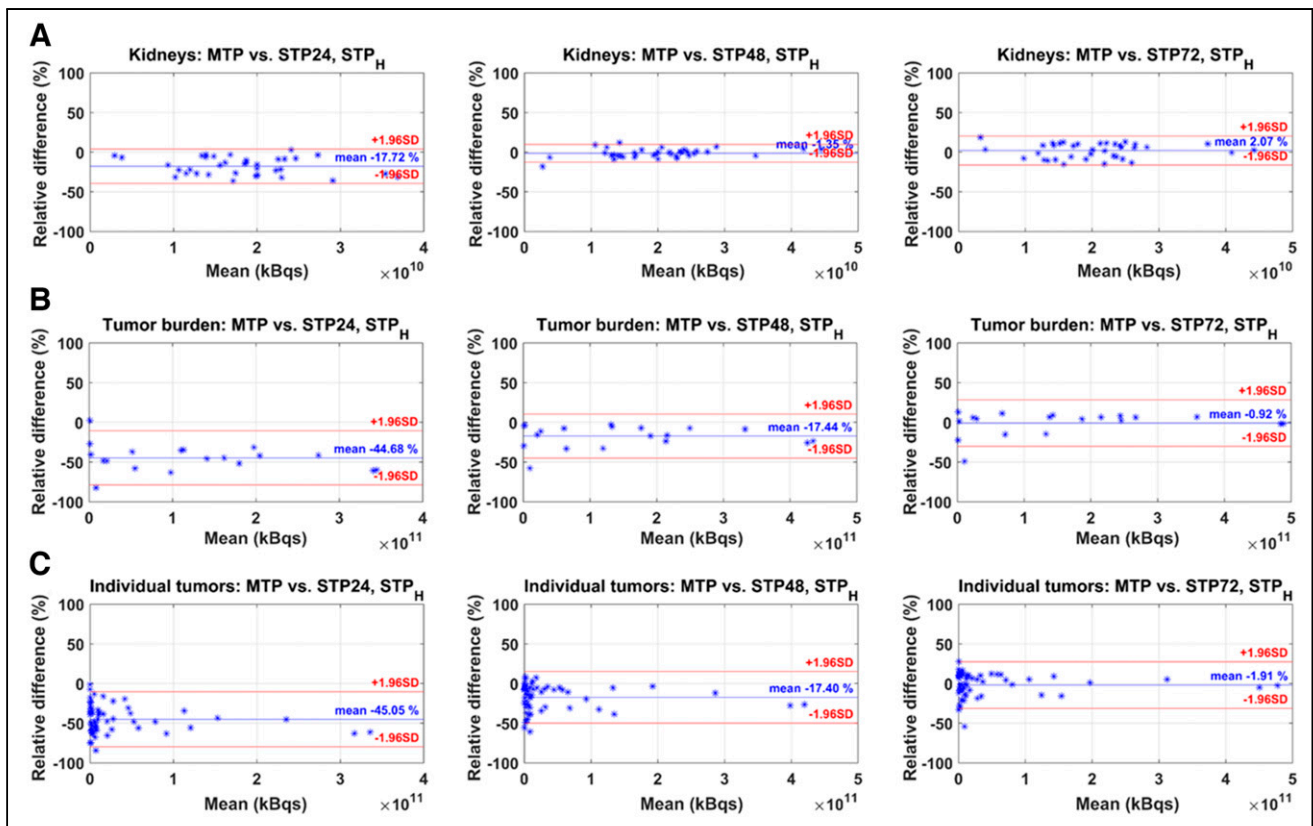


**FIGURE 5.** Bland-Altman plots of STP<sub>H</sub> vs. MTP reference for kidneys (A), TB<sub>FOV</sub> (B), and individual lesions (C). STP24 = STP at 24 h p.i.; STP48 = STP at 48 h p.i.; STP72 = STP at 72 h p.i.

for <sup>177</sup>Lu-PSMA-617 (25), both of whom found better agreement between STP and MTP for lesions at imaging time points even beyond 72 h p.i. STP<sub>H</sub> showed an overall underestimation of TIA for TB<sub>FOV</sub> and individual lesions (Fig. 3B). A similar negative skew for STP<sub>H</sub> was previously observed by Gustafsson and Taprogge (28), underlining that STP approaches are limited in accuracy and that the distribution of T<sub>1/2 eff</sub> in a population must be carefully determined. Our results, however, suggest that STP<sub>prior</sub> is more suitable for tumor dosimetry, especially if the time point is 48 h p.i., matching our recommendation for kidneys. For STP<sub>prior</sub>, it is expected that most TIAs will fall within 20% of those calculated with MTP. Our suggestion of performing SPECT at 48 h p.i. agrees with the analysis of Hou et al. (24). Generally, this recommendation is limited for STP<sub>H</sub>, since, as shown in Table 1, the imaging time point of 48 h p.i. was outside the interval

from 0.75 to 2.5 times the T<sub>1/2 eff</sub> for about 50% of the individual lesions for cycles 1 and 2 and for 50%–60% of TB<sub>FOV</sub>.

The hybrid MTP/STP (STP<sub>prior</sub>) approach presented here allows for collection of all required SPECT images during the routine 3-d hospital stay for patients receiving <sup>177</sup>Lu-PSMA-617 therapy at our institution. This data collection should, however, still be feasible for other institutions with in-patient therapies and for centers that discharge patients on day 0 if they agree to return during the following 2 days. We understand that the latter situation is not optimal, but open communication with the patient highlighting the benefit of MTP imaging during first therapy cycle may increase the patient's willingness to cooperate and participate in multiple scans. When a patient can tolerate only STP imaging (e.g., because of pain) or when only a single scan is feasible due to scanner

**TABLE 1**  
Number of VOIs for Which Imaging Time Point was Within Interval from 0.75 to 2.5 Times T<sub>1/2 eff</sub> of Cycle 1 or 2

Parameter	Cycle	VOIs (n)		
		24 h p.i.	48 h p.i.	72 h p.i.
Kidneys (N = 37)	1	7 (19%)	36 (97%)	28 (76%)
	2	12 (32%)	37 (100%)	27 (73%)
TB <sub>FOV</sub> (N = 19)	1	0 (0%)	6 (32%)	17 (89%)
	2	1 (5%)	9 (47%)	15 (79%)
Individual lesions (N = 56)	1	3 (5%)	26 (46%)	43 (77%)
	2	2 (4%)	30 (54%)	42 (75%)

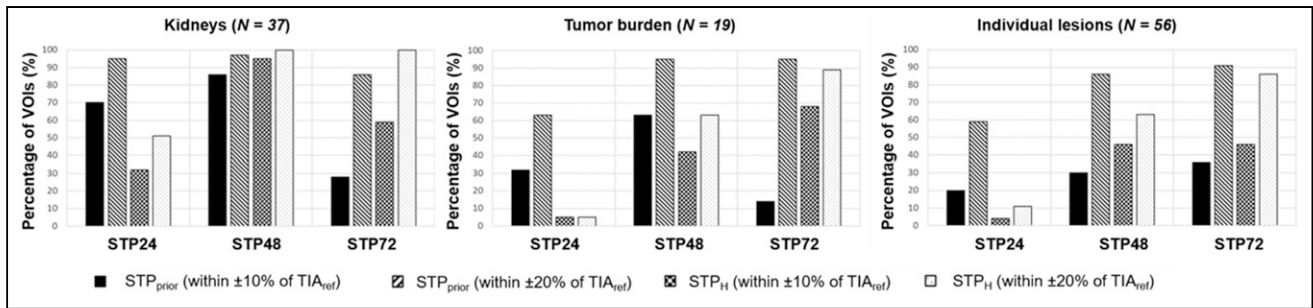


**FIGURE 6.** Percentage of VOIs for which difference in TIA for STP vs. MTP fell within  $\pm 10\%$  or  $\pm 20\%$ .

availability or there are reimbursement issues, the STP<sub>H</sub> approach can still be valid. However, imaging should be performed at 72 h p.i. or later (Fig. 6), when differences in TIA were within  $\pm 20\%$  for all kidneys and for over 85% of the investigated TB<sub>FOV</sub> and individual lesions. In our investigation, this imaging time point was within the interval from 0.75 to 2.5 times the  $T_{1/2\text{ eff}}$  for over 70% of kidneys, TB<sub>FOV</sub>, and individual lesions, as shown in Table 1.

Specific patient situations should be considered when STP methods are applied. The STP<sub>prior</sub> approach may be more prone to deviations from TIA<sub>ref</sub> for lesions in cases of progressive disease or fast response (Supplemental Fig. 1). Protection of healthy organs from radiation-induced toxicities trumps achieving the highest possible lesion doses. When considering the minimum and maximum PDs of  $-21\%$  and  $14\%$  for kidney TIA achieved with an STP<sub>prior</sub> at 48 h p.i., and of  $-18.1\%$  to  $12.1\%$  with STP<sub>H</sub>, these PDs bear the risk of under- or overestimation of the actual kidney dose. Dose underestimation in the individual patient may lead to application of subsequent therapy cycles even if the kidney dose threshold has already been exceeded. ADs obtained from STP methods should therefore be interpreted with caution, in view of the approximately 20% underestimation in a few patients. The condition and kidney function of the individual patient before and during treatment must be closely monitored to prevent radiation-induced toxicity. Our analysis revealed large minimum and maximum PDs of  $-19\%$  to  $33\%$  for TB<sub>FOV</sub> and  $-33\%$  to  $43\%$  for individual lesions for an STP<sub>prior</sub> at 48 h p.i., and of  $-58\%$  to  $-3\%$  for TB<sub>FOV</sub> and  $-61\%$  to  $8\%$  for individual lesions when using STP<sub>H</sub>. Since current clinical practice focuses on protection of healthy organs, these large ranges will likely not influence the patient's course of treatment. However, this variation in lesion AD, with possible over- or underestimation of the actual lesion AD, can potentially impact the derivation of dose–response relationships for prostate cancer lesions. The research community should therefore focus on MTP-derived lesion ADs to determine the response of lesions to <sup>177</sup>Lu-PSMA-617 therapy of prostate cancer. In case the therapeutic scheme for PSMA therapy includes PET/CT staging after every second therapy cycle, this information can be used to guide whether MTP imaging might become necessary for the subsequent therapy cycle because of large changes in tumor burden.

We recognize the limitation that our imaging protocol did not include time points after 72 h p.i. This study was based on the available imaging data at our institution—data that were acquired during the routine 3-d hospital stay for patients receiving <sup>177</sup>Lu-PSMA-617 therapy. However, our ranges of collected imaging time points are comparable to those of other institutions (26,29–31). Further research is needed to assess the validity of our results, including time points of 96 h p.i. or later, and may lead to a different favorable time point for the STP approach for lesions due to their longer retention time

(32) than was shown in our study. Our suggested imaging time point of 48 h p.i. ensured that the TIA determined with STP<sub>prior</sub> was within  $\pm 20\%$  of the TIA<sub>ref</sub> for 97% of kidneys, 95% of TB<sub>FOV</sub>, and 86% of individual lesions (Fig. 6). However, this 48 h p.i. time point is outside the interval from 0.75 to 2.5 times the  $T_{1/2\text{ eff}}$  for about 50% of the individual lesions for cycles 1 and 2 and for 50%–60% of TB<sub>FOV</sub> (Table 1). An imaging time point of 72 h p.i. may be more applicable for STP<sub>H</sub> for lesions but with larger differences from TIA<sub>ref</sub> for kidneys.

Patients with mCRPC may present with extensive metastases which can challenge the tracking of lesions across cycles and the calculation of ADs on an individual-lesion basis. Our analysis for individual lesions was therefore limited to 6 representative lesions per patient. Organ and lesion  $T_{1/2\text{ eff}}$  not only may depend on the individual patient but may vary widely between radiopharmaceuticals (Table 2 of Hou et al. (24) and Fig. 3 of Schuchardt et al. (33)). The applicability of different STP dosimetry approaches should therefore be carefully investigated for different organs, tumors, and radiopharmaceuticals. Future work should include organs that were outside or not entirely within the FOV of our 1-bed SPECT, as well as including all lesions per patient and expanding the analysis to other PSMA compounds. Further studies should investigate how parameters that can be acquired prior to therapy may impact  $T_{1/2\text{ eff}}$ . MTP imaging may be advisable when certain parameters, such as the estimated glomerular filtration rate, are outside the reference range to precisely capture the patient-individual  $T_{1/2\text{ eff}}$ . On the other hand, it can be assessed whether STP approaches are still valid but at different favorable imaging time points. Nevertheless, our results suggest that STP dosimetry is feasible for <sup>177</sup>Lu-PSMA-617 therapies. We hope that these findings simplify dosimetry clinical workflows and ease the implementation of routine dosimetry in RPTs.

## CONCLUSION

The present study assessed STP image-based dosimetry for <sup>177</sup>Lu-PSMA-617 therapy of prostate cancer. Use of a single SPECT/CT scan at 48 or 72 h p.i. after injection of the radiopharmaceutical led to differences from the MTP-based dosimetry that were, overall, within  $\pm 20\%$ . Both STP<sub>H</sub> and STP<sub>prior</sub> were valid for <sup>177</sup>Lu-PSMA-617. Since STP-based dosimetry reduces the burden for patients and the overall costs and complexity of dosimetry, it facilitates the implementation of RPT dosimetry into routine clinical practice.

## DISCLOSURE

This work was partly funded by the German Research Foundation (DFG) within the Research Training Group GRK2274 (Julia

Brosch-Lenz). No other potential conflict of interest relevant to this article was reported.

## KEY POINTS

**QUESTION:** Can the number of imaging time points required for dosimetry be reduced?

**PERTINENT FINDINGS:** STP dosimetry is feasible using either the simplified formula by Hänscheid or a prior information approach that uses MTP imaging for the first therapy cycle with STP imaging for subsequent therapy cycles. Both methods allowed for patient-individual dosimetry for kidneys and lesions, with less than  $\pm 20\%$  PD from MTP-based approaches.

**IMPLICATIONS FOR PATIENT CARE:** Patients will benefit from personalized dosimetry and prediction of related risks and outcome.

## REFERENCES

- Sartor O, de Bono J, Chi KN, et al. Lutetium-177-PSMA-617 for metastatic castration-resistant prostate cancer. *N Engl J Med*. 2021;385:1091–1103.
- Hofman MS, Violet J, Hicks RJ, et al. [ $^{177}\text{Lu}$ ]-PSMA-617 radionuclide treatment in patients with metastatic castration-resistant prostate cancer (LuPSMA trial): a single-centre, single-arm, phase 2 study. *Lancet Oncol*. 2018;19:825–833.
- Baum RP, Kulkarni HR, Schuchardt C, et al.  $^{177}\text{Lu}$ -labeled prostate-specific membrane antigen radioligand therapy of metastatic castration-resistant prostate cancer: safety and efficacy. *J Nucl Med*. 2016;57:1006–1013.
- Ahmadzadehfar H, Rahbar K, Kürpig S, et al. Early side effects and first results of radioligand therapy with  $^{177}\text{Lu}$ -DKFZ-617 PSMA of castrate-resistant metastatic prostate cancer: a two-centre study. *EJNMMI Res*. 2015;5:114.
- Delker A, Fendler WP, Kratochwil C, et al. Dosimetry for  $^{177}\text{Lu}$ -DKFZ-PSMA-617: a new radiopharmaceutical for the treatment of metastatic prostate cancer. *Eur J Nucl Med Mol Imaging*. 2016;43:42–51.
- Garin E, Tselikas L, Guiu B, et al. Personalised versus standard dosimetry approach of selective internal radiation therapy in patients with locally advanced hepatocellular carcinoma (DOSISPHERE-01): a randomised, multicentre, open-label phase 2 trial. *Lancet Gastroenterol Hepatol*. 2021;6:17–29.
- Kratochwil C, Fendler WP, Eiber M, et al. EANM procedure guidelines for radionuclide therapy with  $^{177}\text{Lu}$ -labelled PSMA-ligands ( $^{177}\text{Lu}$ -PSMA-RLT). *Eur J Nucl Med Mol Imaging*. 2019;46:2536–2544.
- Brosch-Lenz J, Yousefirizi F, Zukotynski K, et al. Role of artificial intelligence in theranostics: toward routine personalized radiopharmaceutical therapies. *PET Clin*. 2021;16:627–641.
- Strigari L, Konijnenberg M, Chiesa C, et al. The evidence base for the use of internal dosimetry in the clinical practice of molecular radiotherapy. *Eur J Nucl Med Mol Imaging*. 2014;41:1976–1988.
- Violet J, Jackson P, Ferdinandus J, et al. Dosimetry of  $^{177}\text{Lu}$ -PSMA-617 in metastatic castration-resistant prostate cancer: correlations between pretherapeutic imaging and whole-body tumor dosimetry with treatment outcomes. *J Nucl Med*. 2019;60:517–523.
- Graves SA, Bageac A, Crowley JR, Merlino DAM. Reimbursement approaches for radiopharmaceutical dosimetry: current status and future opportunities. *J Nucl Med*. 2021;62(suppl 3):48S–59S.
- Council directive 2013/59/Euratom of 5 December 2013 laying down basic safety standards for protection against the dangers arising from exposure to ionising radiation, and repealing directives 89/618/Euratom, 90/641/Euratom, 96/29/Euratom, 97/43/Euratom and 2003/122/Euratom. Eur-lex website. <https://eur-lex.europa.eu/eli/dir/2013/59/oj>. Published December 5, 2013. Updated January 17, 2014. Accessed February 1, 2023.
- Hänscheid H, Lapa C, Buck AK, Lassmann M, Werner RA. Dose mapping after endoradiotherapy with  $^{177}\text{Lu}$ -DOTATATE/DOTATOC by a single measurement after 4 days. *J Nucl Med*. 2018;59:75–81.
- Ljungberg M, Celler A, Konijnenberg MW, et al. MIRD pamphlet no. 26: joint EANM/MIRD guidelines for quantitative  $^{177}\text{Lu}$  SPECT applied for dosimetry of radiopharmaceutical therapy. *J Nucl Med*. 2016;57:151–162.
- Uribe CF, Esquinas PL, Tanguay J, et al. Accuracy of  $^{177}\text{Lu}$  activity quantification in SPECT imaging: a phantom study. *EJNMMI Phys*. 2017;4:2.
- Gosewisch A, Delker A, Tattenberg S, et al. Patient-specific image-based bone marrow dosimetry in Lu-177-[DOTA<sup>0</sup>,Tyr<sup>3</sup>]-octreotate and Lu-177-DKFZ-PSMA-617 therapy: investigation of a new hybrid image approach. *EJNMMI Res*. 2018;8:76.
- Brosch-Lenz J, Uribe C, Gosewisch A, et al. Influence of dosimetry method on bone lesion absorbed dose estimates in PSMA therapy: application to mCRPC patients receiving Lu-177-PSMA-I&T. *EJNMMI Phys*. 2021;8:26.
- Gafita A, Bieth M, Krönke M, et al. qPSMA: semiautomatic software for whole-body tumor burden assessment in prostate cancer using  $^{68}\text{Ga}$ -PSMA11 PET/CT. *J Nucl Med*. 2019;60:1277–1283.
- Bland JM, Altman DG. Statistical methods for assessing agreement between two methods of clinical measurement. *Lancet*. 1986;1:307–310.
- Bland JM, Altman DG. Measuring agreement in method comparison studies. *Stat Methods Med Res*. 1999;8:135–160.
- Del Prete M, Arsenault F, Saighi N, et al. Accuracy and reproducibility of simplified QSPECT dosimetry for personalized  $^{177}\text{Lu}$ -octreotate PRRT. *EJNMMI Phys*. 2018;5:25.
- Zhao W, Esquinas PL, Frezza A, Hou X, Beaugard JM, Celler A. Accuracy of kidney dosimetry performed using simplified time activity curve modelling methods: a  $^{177}\text{Lu}$ -DOTATATE patient study. *Phys Med Biol*. 2019;64:175006.
- Willowson KP, Eslick E, Ryu H, Poon A, Bernard EJ, Bailey DL. Feasibility and accuracy of single time point imaging for renal dosimetry following  $^{177}\text{Lu}$ -DOTATATE ('Lutate') therapy. *EJNMMI Phys*. 2018;5:33.
- Hou X, Brosch J, Uribe C, et al. Feasibility of single-time-point dosimetry for radiopharmaceutical therapies. *J Nucl Med*. 2021;62:1006–1011.
- Jackson PA, Hofman MS, Hicks RJ, Scalzo M, Violet J. Radiation dosimetry in  $^{177}\text{Lu}$ -PSMA-617 therapy using a single posttreatment SPECT/CT scan: a novel methodology to generate time- and tissue-specific dose factors. *J Nucl Med*. 2020;61:1030–1036.
- Kurth J, Heuschkel M, Tonn A, et al. Streamlined schemes for dosimetry of  $^{177}\text{Lu}$ -labeled PSMA targeting radioligands in therapy of prostate cancer. *Cancers (Basel)*. 2021;13:3884.
- Madsen MT, Menda Y, O'Dorisio TM, O'Dorisio MS. Technical note: single time point dose estimate for exponential clearance. *Med Phys*. 2018;45:2318–2324.
- Gustafsson J, Taprogge J. Theoretical aspects on the use of single-time-point dosimetry for radionuclide therapy. *Phys Med Biol*. 2022;67.
- Hohberg M, Eschner W, Schmidt M, et al. Lacrimal glands may represent organs at risk for radionuclide therapy of prostate cancer with [ $^{177}\text{Lu}$ ]DKFZ-PSMA-617. *Mol Imaging Biol*. 2016;18:437–445.
- Peters SMB, Privé BM, de Bakker M, et al. Intra-therapeutic dosimetry of [ $^{177}\text{Lu}$ ]Lu-PSMA-617 in low-volume hormone-sensitive metastatic prostate cancer patients and correlation with treatment outcome. *Eur J Nucl Med Mol Imaging*. 2022;49:460–469.
- Privé BM, Peters SMB, Muselaers CHJ, et al. Lutetium-177-PSMA-617 in low-volume hormone-sensitive metastatic prostate cancer: a prospective pilot study. *Clin Cancer Res*. 2021;27:3595–3601.
- Rinscheid A, Kletting P, Eiber M, Beer AJ, Glatting G. Influence of sampling schedules on [ $^{177}\text{Lu}$ ]Lu-PSMA dosimetry. *EJNMMI Phys*. 2020;7:41.
- Schuchardt C, Zhang J, Kulkarni HR, Chen X, Müller D, Baum RP. Prostate-specific membrane antigen radioligand therapy using  $^{177}\text{Lu}$ -PSMA I&T and  $^{177}\text{Lu}$ -PSMA-617 in patients with metastatic castration-resistant prostate cancer: comparison of safety, biodistribution, and dosimetry. *J Nucl Med*. 2022;63:1199–1207.